Generic maximum-valence model for fluid polyamorphism

Nikolay A. Shumovskyi[1] and Sergey V. Buldyrev[1,2,*]

[1]*Department of Physics, Boston University , Boston, Massachusetts 02215, USA*
[2]*Department of Physics, Yeshiva University, New York, New York 10033, USA*

Recently, a maximal-valence model has been proposed to model a liquid-liquid phase transition induced by polymerization in sulfur. In this paper we present a simple generic model to describe liquid polyamorphism in single-component fluids using a maximum-valence approach for any arbitrary coordination number. The model contains three types of interactions: (i) atoms attract each other by van der Waals forces that generate a liquid-gas transition at low pressures, (ii) atoms may form covalent bonds that induce association, and (iii) additional repulsive forces between atoms with maximal valence and atoms with any valence. This additional repulsion generates liquid-liquid phase separation and the region of the negative heat expansion coefficient (density anomaly) on a $P - T$ phase diagram. We show the existence of liquid-liquid phase transitions for dimerization, polymerization, gelation, and network formation for corresponding coordination numbers $z = 1, 2, \ldots, 6$ and discuss the limits of this generic model for producing fluid polyamorphism.

I. INTRODUCTION

The existence of two alternative liquid phases in a single-component substance is known as "liquid polyamorphism" [1–3]. A substance may be found to be polyamorphic by experimentally or computationally detecting a liquid-liquid phase transition (LLPT), which can be terminated at a liquid-liquid critical point (LLCP) [4,5]. Liquid polyamorphism has been observed in a variety of substances, including hydrogen [6–8], helium [9,10], sulfur [11], phosphorous [12,13], and liquid carbon [14], while being proposed to exist in selenium and tellurium [15,16]. It has also been hypothesized in metastable deeply supercooled water below the temperature of spontaneous ice nucleation [1–3,17–25].

The phenomenon of liquid polyamorphism can be understood through the interconversion of the two alternative molecular or supramolecular states via a reversible reaction [2,26,27]. While for some polyamorphic systems, like supercooled water, this approach is still being debated, there are substances (such as hydrogen, sulfur, phosphorous, and liquid carbon) where liquid-liquid phase separation is indeed induced by a chemical reaction. For example, it was recently discovered that high-density sulfur, well above the liquid-gas critical pressure (in the range from 0.5 to 2.0 GPa), exhibits a LLPT indicated by a discontinuity in density from a low-density-liquid (LDL) monomer-rich phase to a high-density-liquid (HDL) polymer-rich phase [11]. This liquid-liquid transition is found in a polymerized state of sulfur (observed above 160 °C at ambient pressure [28–32]). Another liquid-liquid transition accompanied by a reaction has been observed in hydrogen at extremely high pressures (above 325 GPa at ambient temperature [8]), in

which liquid-molecular hydrogen (dimers) dissociates into atomistic-metallic hydrogen [6,7].

In this work, motivated by the recent discoveries of the LLPT in hydrogen [8], and continuing our previous work on the maximal-valence model for sulfur [33], we propose a simple generic model to describe liquid polyamorphism in a variety of chemically reacting fluids. The model combines the ideas of two-state thermodynamics [2,22] with the maximum-valence approach [34–36], in which atoms may form covalent bonds via a reversible reaction, changing their state according to their bond number. By mimicking the valence structure by the maximum bond number z, our model predicts the LLPT in systems with dimerization ($z = 1$), polymerization ($z = 2$), and gelation ($z > 2$). We show that, when the atoms with maximal valence repel atoms with any valence, phase separation is coupled to dimerization ($z = 1$), polymerization ($z = 2$), and gelation ($z > 2$), thus generating the LLPT in polyamorphic substances. The key difference of this paper and the previously published one [33] is that here we investigate the case of *repulsion* between atoms with the maximum valence z and any other atoms, which causes the segregation of the atoms with the maximum valence into the *low*-density phase; while in the previous paper, in which we attempted to model sulfur, we investigate the case of *attraction* of the atoms of maximal valence ($z = 2$) to each other, which causes segregation of the polymerized atoms into the *high*-density phase. Thus we have two classes of maximal-valence models—one with attraction and another with repulsion—which drastically differ from each other. The models with repulsion studied here do have a density anomaly region with a negative heat expansion coefficient of $\alpha_P < 0$, while the models with attraction do not.

II. MAXIMUM-VALENCE MODEL

We model LLPT induced by molecular interconversion in polyamorphic substances by characterizing each atom by its
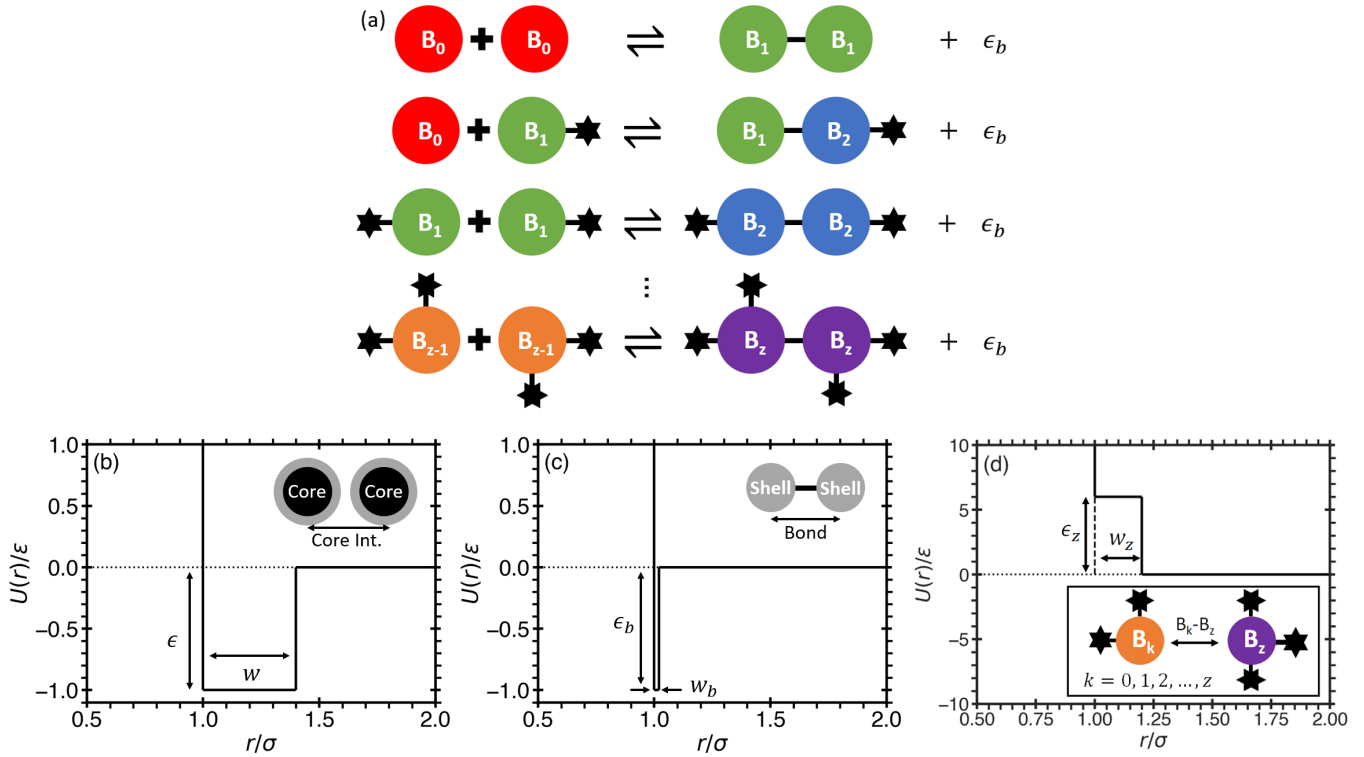
---

*buldyrev@yu.edu

FIG. 1. Reactions and interactions in the generic maximum-valence model with repulsion. (a) $z(z+1)/2$ types of covalent-bond-forming reversible chemical reactions that may occur in the system. If two atoms without bonds (B_0) collide with each other, they may form a bond and become B_1 atoms. If a B_0 atom and a B_1 atom collide, they may form a bond and become B_1 and B_2 atoms, respectively. If two B_1 atoms collide with each other, they form an additional bond and become B_2 atoms. This continues until the atoms reach their maximum valency—state B_z. (b)–(d) The three major interactions between atoms, in which each atom is composed of a core and a shell, both with a diameter σ and a mass m. $U(r)$ is the pair potential energy and r is the distance between the centers of the particles. (b) The cores of each atom interact with an attractive square well of depth ϵ and width w. (c) The shells may react to form covalent bonds that consist of a narrow well with depth ϵ_b and width w_b. (d) Phase segregation is coupled to dimerization, polymerization, gelation, etc., via the additional repulsive interactions between atoms in state B_z and atoms in state B_k with $k \leqslant z$, described by a square shoulder of height $-\epsilon_z$ and width w_z.

coordination number $k \leqslant z$, the number of bonds it has with other atoms. Depending on the coordination number, each atom is assigned to distinguished $z + 1$ states: B_0 (with zero bonds), B_1 (with one bond), B_k (with k bonds), and finally B_z (with z bonds). Atoms cannot form more than z bonds and, consequently, will associate into either dimers, for $z = 1$, or linear polymers, $z = 2$, or some network structure $z > 2$. All of the atoms in the system may change their state by forming or breaking a covalent bond via a reversible reaction. Figure 1(a) depicts all $z(z + 1)/2$ types of reversible reactions that may occur in the system. In this work, we demonstrate that the minimum ingredients required to produce a LLPT are the following: (i) the van der Waals interactions between atoms, which produce a liquid-gas phase transition; (ii) covalent bonds between atoms, which induce association; and (iii), as we hypothesize, additional repulsive interactions between atoms with maximum valence ($k = z$) and atoms with any valence ($k \leqslant z$), which are needed to couple phase segregation to dimerization, polymerization, or gelation. These three ingredients are illustrated by square-well potentials in Figs. 1(b)–(d).

In the case of hydrogen, the pioneering quantum calculations of Wigner and Huntington [37] suggested that at high density the energy of the metallic lattice is lower than the energy of the molecular lattice. In other words, at high densities

H_2 dimers disassociate due to a steric effect; i.e., the electron shells of H_2 dimers are getting larger than the intermolecular distances. This steric repulsion is expected to happen not only for the case of hydrogen but also for other molecular liquids with higher valence.

A similar rule may be applied to the case of water. It was found experimentally that, at high densities when the fifth neighbors are being pushed into the first coordination shell of a molecule, hydrogen bonds bifurcate and the energy of the bifurcated bonds are roughly half of the energy of the straight bonds [38]. Essentially this implies that the shells of the atoms with coordination number 4 become impenetrable for a fifth intruder at low temperatures.

To verify our hypothesis, we implement these three ingredients of interactions via an event-driven molecular dynamics (MD) technique [39,40]; in particular, we use a discrete MD package that only includes particles interacting through spherically symmetric stepwise potentials, which may form bonds via reversible reactions [41]. We simulate an NVT ensemble of $N = 1000$ atoms in a cubic box with periodic boundaries at various constant densities and temperatures. The temperature is controlled by a Berendsen thermostat [42]. The van der Waals and covalent-bonding interactions are implemented by separating each atom into two overlapping hard spheres (a core and a shell), with the same diameter σ and mass m

[see Figs. 1(b)–(d)]. The connection between the core and its shell is represented by an infinite square-well potential of width $d \ll \sigma$. The cores and shells of different atoms do not interact with each other. The core represents the atom without its valence electrons. It interacts with other cores via a wide potential well with depth ϵ and width $w \sim \sigma$. We use σ, m, and ϵ as units of length, mass, and energy, respectively, and measure all other physical quantities using a combination of these units. For example, the temperature T is measured in units of ϵ/k_B where k_B is the Boltzmann constant, the pressure P is measured in units of ϵ/σ^3; and the time t is measured in units of $\sigma\sqrt{m/\epsilon}$. We note that all physical parameters reported below are normalized by the appropriate combination of mass m, length σ, and energy ϵ units, as used in Ref. [43]. Meanwhile, the shell represents the outer valence electron cloud. It can form bonds with other shells via a narrow potential well with depth $\epsilon_b = \epsilon$ and width w_b [Fig. 1(c)], which models the breaking and forming of covalent bonds. When the shell interactions are included and the system may form covalent bonds, the location of the liquid-gas critical point (LGCP) changes, but not significantly. Note that, for $z \geqslant 3$, the liquid-gas critical point may form due to bonds only without van der Waals attraction between the cores as in the original maximal-valence model [34]. Also we introduce an additional repulsive potential shoulder [with depth ϵ_z and width w_z, Fig. 1(d)] to model the steric repulsion of the atoms with z bonds, which are not chemically bonded to each other. Here we assume that $\epsilon_z < 0$ means repulsion, while $\epsilon_z > 0$ means attraction. We also emphasize the key difference between the case of repulsion in this work and attraction for the atoms of the maximal-valence model for sulfur [33]. In the case of attraction, the shells in the state B_z attract each other, but do not interact with other shells other than by hard-core repulsion with diameter σ. Conversely, for the case of repulsion, shells in the state B_z repel from each other and from all other shells, while other shells do not interact with each other except by forming and breaking bonds, with the condition that two nonbonded atoms with $k < z$ cannot be within a distance of each other smaller than the bond length w_b. Technically, this is achieved by assigning to such a pair a very strong repulsive potential at distance w_b.

We note that during either the formation or the breaking of a bond, the new state of the reacting particles may modify the potential energy of their interactions with their nonbonded neighboring particles. In our model, this occurs when particles in the state B_k convert to the state B_{k-1} (or vice versa). To maintain the conservation of energy, we calculate the change of the total potential energy, ΔU, due to the change of the state of the reacting particles, and subtract it from the kinetic energy of the reacting pair. As a consequence, the equations for computing the new velocities [41] may not have real solutions. In this case, the bond will not form or break, and the reacting particles will conserve their states through an elastic collision.

The applicability of the maximum-valence model has been already tested for the case of sulfur ($z = 2$, $\epsilon_z > 0$) [33]. Here we focus on an arbitrary value of z and additional repulsive interactions $\epsilon_z < 0$. Note that for the case of attraction ($\epsilon_z > 0$) the high density phase is polymerized. In the case of repulsion, $\epsilon_z < 0$, the low-density phase is dimerized, is polymerized, or
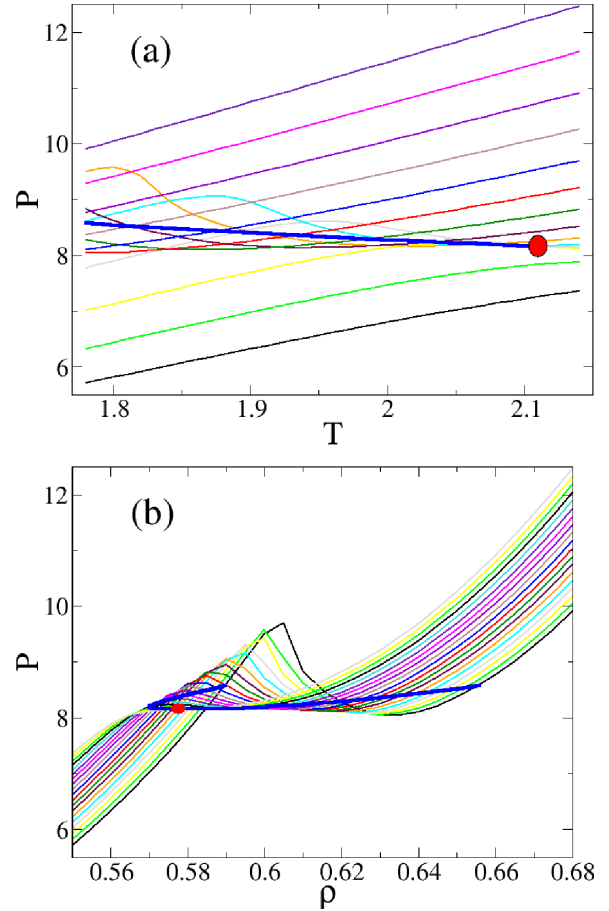

FIG. 2. Phase diagrams for the maximum-valence model of dimerization, $z = 1$ ($w_b = 0.10$, $w = 0.5$, $w_z = 0.2$, $\epsilon_b = 6$, $\epsilon_z = -12$), obtained in an NVT ensemble after $t = 10^6$ time units. (a) The isochores in the $P - T$ plane with $\rho = 0.550$–0.680 in steps $\Delta\rho = 0.005$. (b) The isotherms in the $P - \rho$ plane with $T = 1.78 - 2.14$ in steps $\Delta T = 0.01$. In both figures, the liquid-liquid coexistence curves are calculated via the Maxwell construction and indicated by the blue curves. The liquid-liquid ($T_c^{LL} = 2.12$, $P_c^{LL} = 8.1655$, $\rho_c^{LL} = 0.5775$) critical point is indicated by the red circles.

forms a network with the coordination number z. By tuning z, the phase behavior of a variety of substances can be described. For instance, for $z = 1$, dimerization-induced phase separation (such as in high-pressure hydrogen [6–8]) is investigated, while for $z > 2$, gelation-induced phase separation is investigated. In particular, the phase behavior of more complex chemically reacting systems, such as phosphorous ($z = 3$) [12,13] and supercooled water, forming hydrogen instead of covalent bonds, ($z > 3$)$^{18-32,34,35}$, can be investigated.

III. DIMERIZATION ($Z = 1$)

We start with the simplest case of $z = 1$, i.e., dimerization. We are allowing our system to have only two types of atoms, B_0 and B_1, which interact and may react by the scheme described by Fig. 1 with the maximal valence $z = 1$. We found that in the case of repulsion between the atoms with the maximal valence B_1, we see liquid-liquid phase transition produced by dimerization of atoms while reducing

pressure. To mimic the behavior of the hydrogen we select the following set of parameters: $w = 0.5$, $w_b = 0.1$, $\epsilon_b = 6$, $w_1 = 0.2$, and $\epsilon_1 = -12$. The choice of very large values of ϵ_b and ϵ_z, compared to ϵ of the van der Waals forces, is motivated by the desire to make the temperature and the pressure of the LGCP much smaller than the temperature and the pressure of the LLCP. For the selected set of parameters, the LGCP is located at $T_c^{LG} = 0.91 \pm 0.02$, $P_c^{LG} = 0.030 \pm 0.002$, and $\rho_c^{LG} = 0.225 \pm 0.005$. Figure 2(a) shows the $P - T$ phase diagram for this set of parameters near the LLCP with the crossing of isochores at $T_c^{LL} = 2.12$, $P_c^{LL} = 8.1655$, and $\rho_c^{LL} = 0.5775$; the liquid-liquid coexistence line is shown by the blue line ending in the LLCP marked with a red ellipse. Note that in the region near the critical point the slopes of the isochores become negative, which means that there exists a region of density anomaly in which the density of the liquid decreases upon cooling. Moreover, it may indicate that the critical point is located in the region of density anomaly, which implies that the critical isochores and the liquid-liquid coexistence line have a negative slope. Figure 2(b) shows the apparent van der Waals loops on the $P - \rho$ phase diagram, which correspond to the liquid-liquid phase transition.

Another interesting feature of the model is found by looking at the temperature-density phase diagram, as well as the plot of temperature vs fraction of bonded atoms $\phi = N_1/N$, where N is the total number of atoms and N_1 is the number of atoms in state B_1. In these diagrams we used reduced variables $\phi_r = (\phi - \phi_c)/\phi_c$, $T_r = (T - T_c)/T_c$, and $\rho_r = (\rho - \rho_c)/\rho_c$, with $\rho_c = 0.5775$, $T_c = 2.12$, and $\phi_c = 0.350$ for $w_b = 0.10$ and $\rho_c = 0.76$, $T_c = 2.14434$, and $\phi_c = 0.578$ for $w_b = 0.06$. Figure 3 shows that, while the coexistence line on the $T_r - \rho_r$ phase diagram is highly skewed to the right, the coexistence line on the $T_r - \phi_r$ phase diagram is quite symmetric, which resembles the actual liquid-liquid coexistence line in hydrogen [44]. Note that one might apply a two-state thermodynamics approach and compare the exact solution for hydrogen with our results from the simulations. This comparison is one of our future works in progress which requires a thorough analysis of the hydrogen system.

Next, we studied the dependence of the phase diagram on the parameters ϵ_1 and w_b, the strength of the additional interaction between the atoms in states with maximal valence, i.e., B_1 with $z = 1$, and the width of the bonds. As can be seen in Fig. 4, upon increasing the strength ϵ_1 all the LLCP parameters decrease—critical temperature, critical pressure, and critical density. Physically, it means that, upon increasing the repulsive energy between the bonded atoms, we effectively make the bonds less stable, and hence the temperature must be reduced to increase the stability of the bonds necessary for the liquid-liquid phase segregation. As the repulsive energy between dimers increases, the dimers get less penetrable, and their density, as well as the pressure required to create such a density, drops. Thus we expect that both the density and the pressure of the second critical point decrease as the repulsive energy increases. Figure 4(d) shows that we can force our system to have a negative slope of a liquid-liquid coexistence line on a $P - T$ phase diagram by increasing $|\epsilon_1|$, which qualitatively reproduces the negative slope in real hydrogen. Another important note is that, upon increasing further the
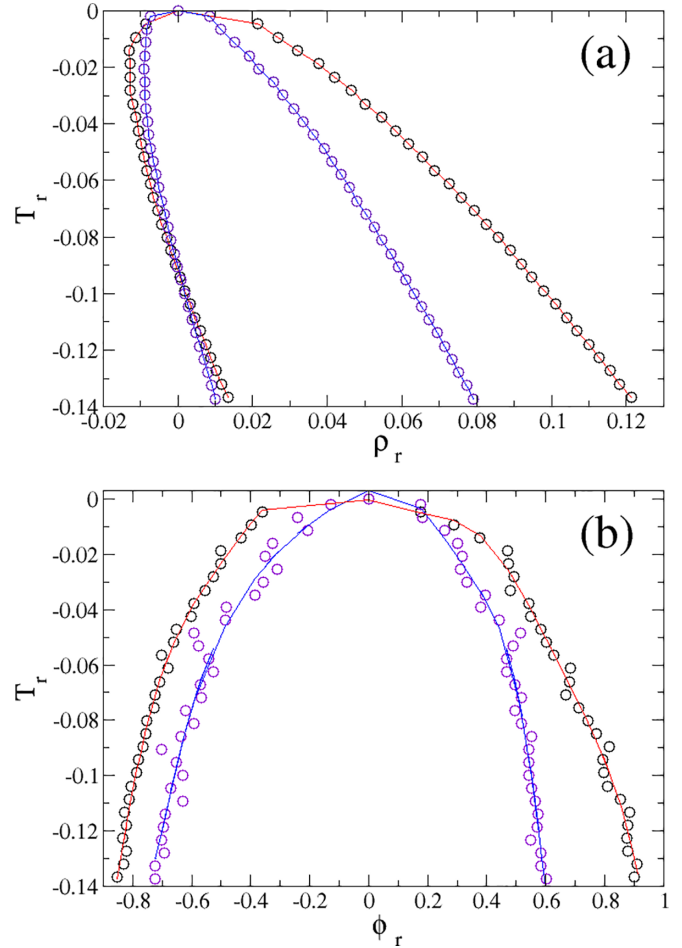

FIG. 3. (a) $T_r - \rho_r$ phase diagram for the maximum-valence model for dimerization, $z = 1$ (with $w_b = 0.10$, red line, and $w_b = 0.06$, blue line), obtained in an NVT ensemble after $t = 10^6$ time units. (b) The reduced temperature dependence of the reduced fraction of atoms with one bond, ϕ_r, in two coexisting liquid phases.
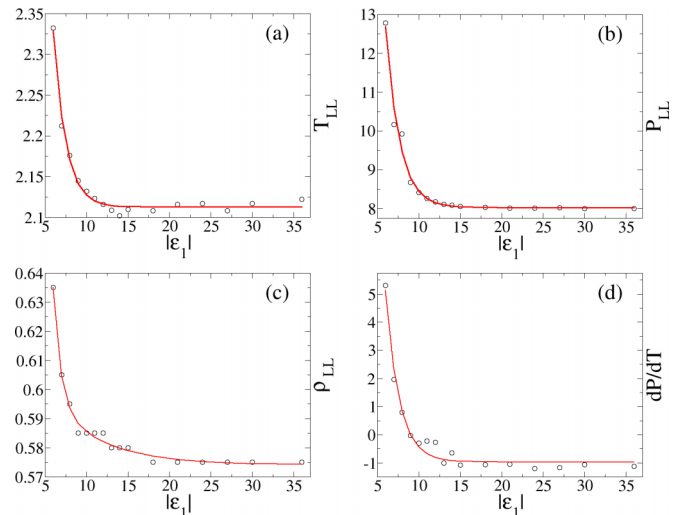

FIG. 4. The dependence of the liquid-liquid critical point parameters on the additional interaction strength $|\epsilon_1|$ for $z = 1$, $w = 0.5$, $d = 0.1$, $w_b = 0.1$, $w_1 = 0.2$, and $\epsilon_b = 6$.
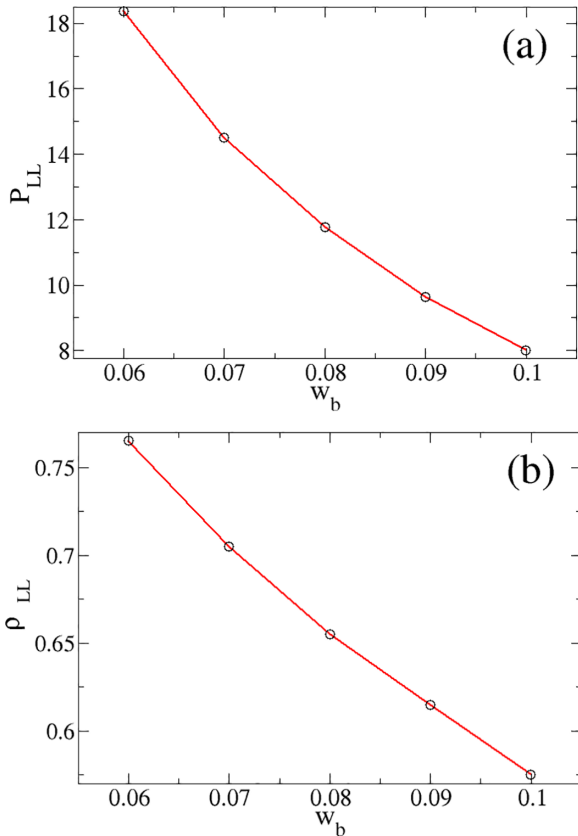
FIG. 5. The dependence of the liquid-liquid critical point parameters on the bond width for $z = 1$, $\epsilon_1 = -12$, $w = 0.5$, $d = 0.1$, $\epsilon_b = 6$, and $w_1 = 2w_b$.
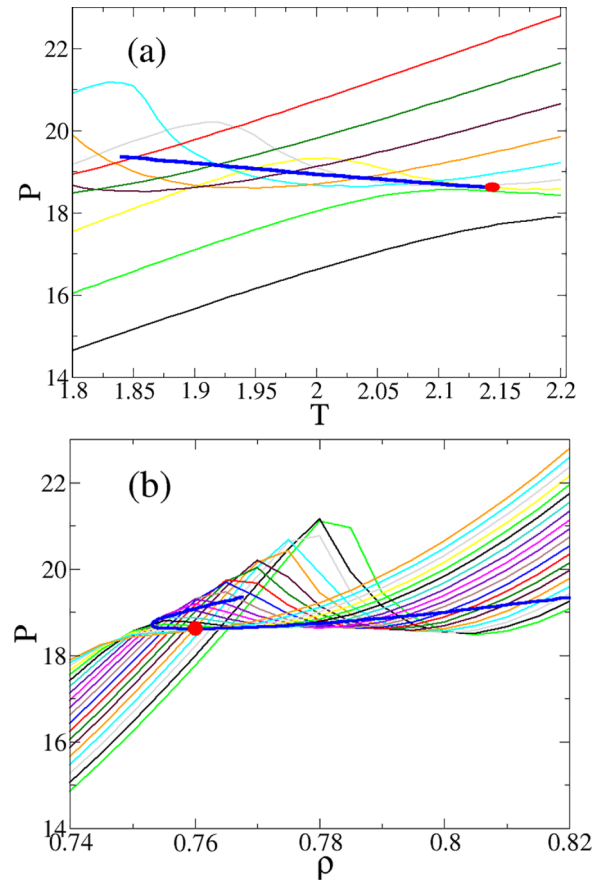

FIG. 6. Phase diagrams for the maximum-valence model of dimerization, $z = 1$ ($w_b = 0.06$), obtained in an NVT ensemble after $t = 10^6$ time units. (a) The isochores in the $P - T$ plane are $\rho = 0.96$–1.20 for $\rho = 0.760$–0.820 in steps $\Delta T = 0.01$. (b) The isotherms in the $P - \rho$ plane for $T = 1.82$–2.20 in steps $\Delta T = 0.01$. In both figures, the liquid-liquid coexistence curves are calculated via the Maxwell construction and indicated by the blue curves. The liquid-liquid ($T_c^{LL} = 2.14434$, $P_c^{LL} = 18.618$, $\rho_c^{LL} = 0.670$) critical point is indicated by the red circles. Other parameters are the same as those in Fig. 5.

interaction energy between atoms with maximal valence, all four plots reach the plateau which corresponds to the limit $|\epsilon_1|/\epsilon_b \to \infty$, when the repulsion strength between B_1 atoms is much larger than the bond strength, the system reaches the limit when the dimers become effectively impenetrable, so the system behaves like a system of quasihard spheres made of dimers which have larger effective radius than hydrogen monomers. The LLCP parameters and the slope of the coexistence line rapidly acquire the values corresponding to this limiting case, because the probability to find an atom sitting on a repulsive shoulder decreases according to Arhenius law $\exp[\epsilon_1/(k_B T)]$. Indeed, all four parameters approach their limit exponentially with $\epsilon_1 \to -\infty$. The limit $\epsilon_1 \to -\infty$ corresponds to the impenetrable electron shells of the H_2 molecules, which cannot exist if another atom enters their electron shells and the molecule must break if such an event happens.

Figure 5 shows the dependence of the liquid-liquid critical pressure and the critical density on the bond width at $\epsilon_b = 6$ and $\epsilon_1 = -12$, keeping $w_1 = 2w_b$: as we increase the bond width, the system does not require that much pressure, or does not need to be in such a squeezed state, for monomers to start dimerization, so the LLCP moves down in both the P and ρ axes; however, the temperature of LLCP stays approximately the same, since the increase of the bond width only plays the entropic effect, not the energetic one. We note that upon decreasing the bond width further below $w = 0.06$, the LLCP

becomes submerged below the crystallization line, and the phase transition is not observed anymore. However, increasing the bond width further will only decrease (P_c, ρ_c) further, up to the point when the liquid-liquid critical pressure becomes negative or the LLCP is getting destroyed by the liquid-gas spinodal. The phase diagrams corresponding to $w_b = 0.06$ are show in Fig. 6.

Note that, when we compare the $T - \rho$ phase diagrams, as well as the plots of $T - \phi$, for the two values of the bond width $w_b = 0.10$ and $w_b = 0.06$, we find that the the coexistence regions are indeed squeezed when we reduce w_b from $w_b = 0.10$ to $w_b = 0.06$. The percentage difference of the densities of the HDL and the LDL far away from the critical point is about 11.5% for $w_b = 0.10$, while for $w_b = 0.06$ it is 6.9% (see Fig. 3). Note that in hydrogen it is approximately 2% [44]. In theory, upon decreasing the bond width we should obtain the desired 2%; however, our simulations show that below $w_b = 0.06$ the LLCP is submerged below the crystallization line.

The same effect can be achieved by reducing the width of repulsive interactions w_1, while keeping w_b constant. The difference in densities decreases when $(w_1 - w_b)/\sigma$ decreases and reaches 6% when $(w_1 - w_b)/\sigma = 0.06$, but further decrease leads to instantaneous crystallization in the region where the LLCP would be expected.

IV. $Z = 2, 3, 4, 5,$ and 6 (POLYMERIZATION, GELATION/NETWORK FORMATION)

We can generalize our model for any arbitrary coordination number z. So far we have discussed in detail only dimerization, $z = 1$, and polymerization, $z = 2$, for attractive interaction between B_2 atoms [33]. Upon studying other $z > 2$, we found that our generic maximal-valence model also produces liquid-liquid phase transitions induced by molecular interconversion in polyamorphic substances for higher z as well, up to the point when the critical density becomes so high that the LLCP moves below the crystallization line.

Figure 7 shows the dependence of critical parameters, critical temperature T_c, critical pressure P_c, and critical density ρ_c, on the coordination number z, while keeping all other parameters constant ($w = 0.5$, $w_b = 0.1$, $w_z = 0.2$, $d = 0.1$, $\epsilon_b = 6$, $\epsilon_z = -6$). Upon increasing z the liquid-liquid critical temperature decreases, while the liquid-gas critical temperature increases. Physically the temperature of the LGCP increases upon increasing the coordination number z, because the overall attraction increases. However, as z increases, both LG and LL critical pressures increase. We know that since T_c^{LG} is increasing, it forces the pressure of liquid-gas also to increase. As for the density of the LGCP, it only slightly increases for high z. On the other hand, the density of the LLCP increases from approximately 0.6 to 1. This is because the density of the low-density phase, which consists of atoms with the coordination number z, increases with z at a constant bond length. When $z = 6$ the network density coincides with the density of the simple cubic lattice which has the coordination number 6. For higher z the LLPT becomes submerged below the crystallization line of the body-centered-cubic lattice. The pressure needed to create such a density also increases, so we see that the LLCP pressure increases with z. The most intriguing observation of Fig. 7(a) is the apparent crossing of the temperatures of the LGCP and the LLCP as z increases. This is in agreement with the experimental observations that for hydrogen ($z = 1$) the liquid-gas critical temperature (33 K) is much smaller than the hypothetical critical temperature of the liquid-liquid critical point (>400 K), while for water ($z = 4$) the liquid-gas critical temperature is 647 K, which is much larger than the hypothetical critical point of the supercooled water, $T < 230$ K. Note that the pressures for the LGCP and the LLCP are quite different, the latter is orders of magnitude larger than the former, so the physical processes behind these critical points are quite independent. The crossing of the critical temperature curves at a particular z is just a coincidence, an interplay of the parameters. What is important is that T_c^{LG} is increasing, while T_c^{LL} is decreasing. While the increase of T_c^{LG} is obvious because for larger z the energy of the liquid phase decreases due to formation of extra bonds, the decrease of T_c^{LL} with z can be explained by the entropic effect. Increasing the number of neighbors in the coordination shell from $z - 1$ to z leads to a larger entropy loss for larger z. This observation
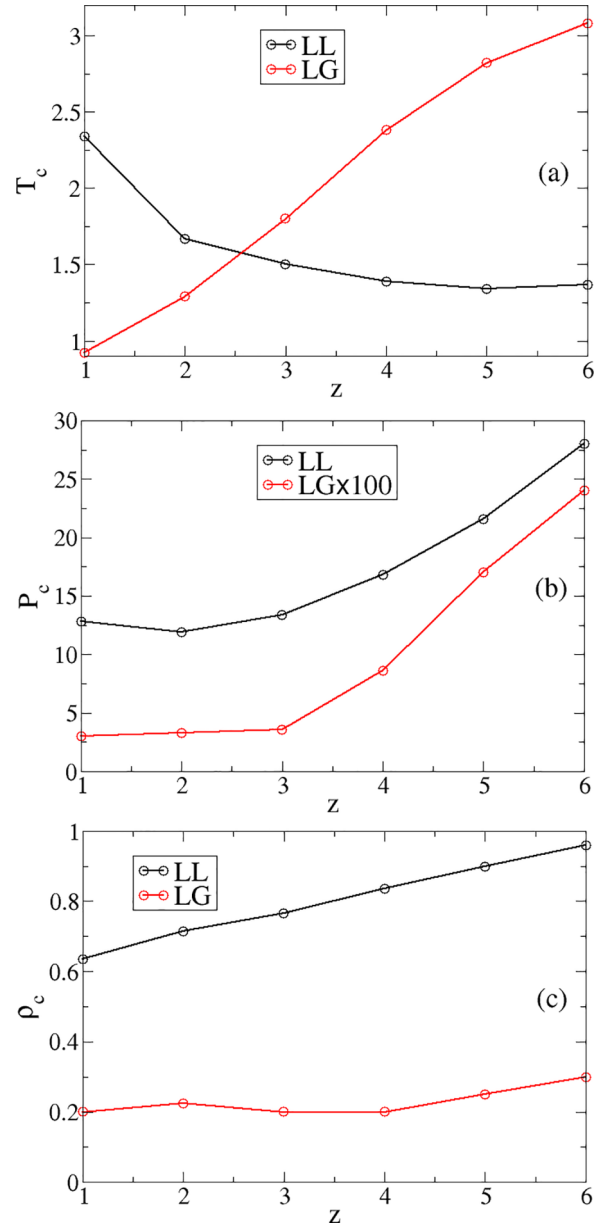

FIG. 7. The dependence of the liquid-liquid critical point parameters on coordination number z. The parameters are $w = 0.5$, $w_b = 0.1$, $w_z = 0.2$, $d = 0.1$, $\epsilon_b = 6$, and $\epsilon_z = -6$.

is consistent with the behavior of the slope of the LL coexistence versus z (Fig. 8). Indeed, for all other parameters being equal, the LL coexistence line for $z = 1$ has a positive slope on a $P - T$ diagram, while for $z \geqslant 2$ the slope is negative and is getting more negative for higher z. This means that the low-density phase for $z = 1$ (dimeric) has higher entropy than the low-density phase (monomeric). In contrast, for $z = 2$ the low-density phase (polymeric) has lower entropy than the high-density phase (dimeric) and for higher values of z this difference is getting more negative. If the heat expansion coefficient is positive, the density and the entropy are negatively correlated, but for negative heat expansion (density anomaly) the density and the entropy are positively correlated [18]. This implies that the higher-density phase has a more disordered neighborhood than the low-density phase. And this
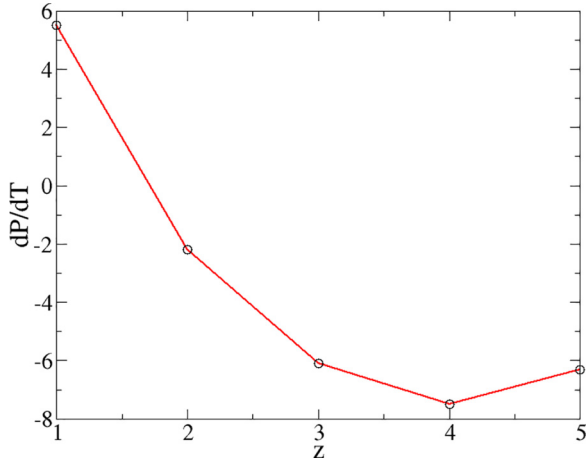
FIG. 8. The dependence of the slope of the liquid-liquid coexistence line on coordination number z. The parameters are $w = 0.5$, $w_b = 0.1$, $w_z = 0.2$, $d = 0.1$, $\epsilon_b = 6$, and $\epsilon_z = -6$.

disordering upon compression increases with z. Thus, analyzing the slope of the coexistence line leads to the same conclusion as analyzing the decrease of the critical temperature with z.

The choice of parameters for our model is quite simple and natural. In reality, a wide region in the parameter space produces a phase diagram with a region of density anomaly and a LLCP with a negatively sloped coexistence line, like it happens in water [21]. In the previous section we find that for $z = 1$ the slope of the coexistence line is negative only for large additional repulsive interaction for the dimerized atoms $\epsilon_1 \approx -2\epsilon_b$. For larger z the the slope becomes negative even for weaker repulsion $\epsilon_z = -\epsilon_b$ (Fig. 8). Our preliminary results show that increasing the width of the repulsive shoulder (w_z) to 1.35 at $z = 4$ while keeping all other parameters constant, as in Fig 7, reduces the pressure of the region of the density anomaly to zero like in water. In this case the critical point is located at negative pressures very close to the LG spinodal. Further increase of w_z leads to the disappearance of the critical point below the LG spinodal, similar to the critical point free scenario [18,45].

Reducing the width to 0.15 leads to the disappearance of the density anomaly together with the critical point. Increasing the height of the shoulder to infinity does not change the phase diagram after a certain point, approximately $|\epsilon_z|/\epsilon_b > 2$, while the decrease of the height to $\epsilon_b/2$ eliminates the critical point. The detailed investigation of the phase diagram for the wide shoulder is very important for understanding the phase diagram of water and is the subject of our current work.

Lastly, Fig. 9 shows the radial distribution function $g(r)$ and the structure factor $S(q)$ for the system with a repulsive interaction for $z = 4$ with the set of parameters $w = 0.5$, $w_b = 0.1$, $w_z = 0.2$, $d = 0.1$, $\epsilon_b = 6$, and $\epsilon_z = -6$ along the isochore $\rho = 0.87$, which crosses the line of the liquid-liquid phase transition illustrated by three snapshots at $T = 1.35$ (high-density phase), $T = 1.09$ (coexistence), and $T = 0.86$ (low-density phase). In the $g(r)$ and $S(q)$ plots for low temperature, one can see the splitting of the first shell into two peaks: the first peak corresponds to the atoms with maximal
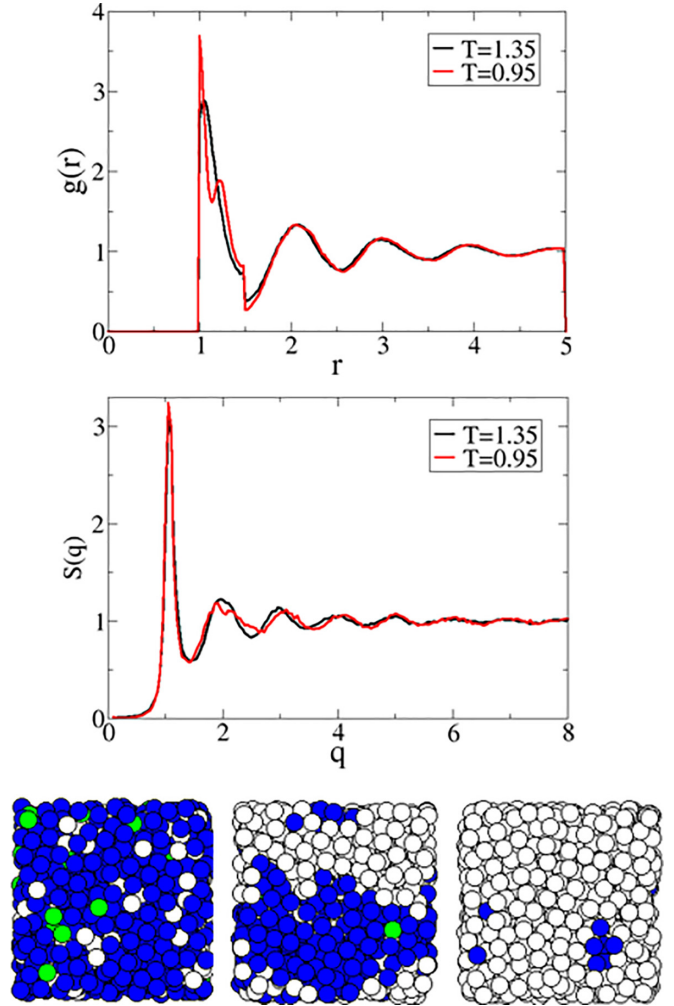

FIG. 9. Radial g factor, $g(r)$, and structure factor, $S(q)$, for the $z = 4$ system with repulsion. The parameters are $w = 0.5$, $w_b = 0.1$, $w_z = 0.2$, $d = 0.1$, $\epsilon_b = 6$, and $\epsilon_z = -6$. The snapshots of the system are presented for $T = 1.35$, $T = 1.09$, and $T = 0.86$ (left to right).

valence ($z = 4$), while the second peak corresponds to the atoms which cannot penetrate into the repulsive shoulder. At low temperatures, we can see the low-density phase consists predominantly of atoms with four bounds (white), while at high temperature we see the high-density phase consists of atoms with three bonds (blue) and of a small fraction of atoms with four bonds (white) and two bonds (green). To relate this picture to the structure of water, we must emphasize that only straight hydrogen bonds are counted as bonds in the maximal-valence model. The bifurcated bonds are counted as the intruders onto the repulsive shoulder with the correspondent energy penalty.

V. CONCLUSION

The maximum-valence model describes liquid polyamorphism in a variety of chemically reacting fluids. By tuning the maximum valency, z (maximum coordination number), of the model, the liquid-liquid phase transitions (LLPT) in these systems can be investigated. We showed that, when the

atoms with maximal valence $k = z$ repel atoms with valence $k \leqslant z$, the LLPT is generated by the coupling between phase separation and the chemical reactions.

We showed that, when $z = 1$, the LLPT is induced by dimerization (e.g., hydrogen at extremely large pressures [8]). We described how, by tuning the size of the molecule relatively to the atomic hydrogen radius, our model may be used to reproduce the real hydrogen. By decreasing the difference between the bond length w_b and the repulsive range of the atoms in the molecule, w_1, one can reduce the relative difference between the densities of high- and low-density phases to 6%, while in the real hydrogen this difference is reported to be approximately 2% [44]. After reducing the difference between w_b and w_1 even further, the system crystallizes. Since the exact position of the LLCP in hydrogen is still under debate [44], our results suggest that 2% difference between high- and low-density phases is inconsistent with the existence of the LLPT above the crystallization line.

In our previous work for $z = 2$, we showed that the LLPT induced by polymerization could describe the LLPT in sulfur [33]. For $z \geqslant 3$, the LLPT could be induced either by gelation or by molecular network formation [34]. For example, it could be used to model the phase behavior of liquid phosphorous with $z = 3$ [12,13] or supercooled water with $z > 3$ [18,36]. Indeed for high values of z we obtained the negative slope of the coexistence line on the $P - T$ plane as well as the relationships between the critical parameters of the model, $T_c^{\mathrm{LG}} \gg T_c^{\mathrm{LL}}$ and $P_c^{\mathrm{LG}} \ll P_c^{\mathrm{LL}}$, which qualitatively reproduces the real water experiments [46] and simulations of more accurate all-atom models.

An interesting question is the existence of the liquid-liquid transition for very high values of z. The highest possible z for short bonds is 12, when the spherical atoms must form the hexagonal-close-packed lattice or the face-centered-cubic lattice. But already, for $z = 6$, the structure of the liquid must resemble a simple cubic lattice, and the liquid becomes prone to crystallization. However, the liquid phase with $z = 6$ can still be observed in a very narrow range of densities. For $z > 6$, the liquid at high densities, necessary to achieve these high coordination numbers, spontaneously crystallizes into the body centered cubic (bcc) lattice, which has the coordination number 8. Our preliminary observations suggest that these bcc crystals may display an isostructural solid-solid phase transition ending in a solid-solid critical point [47].

In a future study, the two-state thermodynamics of liquid polyamorphism [2,26,27,44] could be applied to these systems to develop the equation of state, which would determine the anomalies of the physical properties in these systems, especially near the critical points.

[1] H. E. Stanley, Editor, *Liquid Polymorphism*, Advances in Chemical Physics, Vol. 152 (Wiley & Sons, New York, 2013).

[2] M. A. Anisimov, M. Duška, F. Caupin, L. E. Amrhein, A. Rosenbaum, and R. J. Sadus, Thermodynamics of Fluid Polyamorphism, Phys. Rev. X **8**, 011004 (2018).

[3] H. Tanaka, Liquid–liquid transition and polyamorphism, J. Chem. Phys. **153**, 130901 (2020).

[4] G. Franzese, G. Malescio, A. Skibinsky, S. V. Buldyrev, and H. E. Stanley, Generic mechanism for generating a liquid-liquid phase transition, Nature (London) **409**, 692 (2001).

[5] F. Sciortino, Liquid–liquid transitions: Silicon in silico, Nat. Phys. **7**, 523 (2011).

[6] M. A. Morales, C. Pierleoni, E. Schwegler, and D. M. Ceperley, Evidence for a first-order liquid-liquid transition in high-pressure hydrogen from ab initio simulations, Proc. Natl. Acad. Sci. USA **107**, 12799 (2010).

[7] M. Zaghoo, A. Salamat, and I. F. Silvera, Evidence of a first-order phase transition to metallic hydrogen, Phys. Rev. B **93**, 155128 (2016).

[8] P. Dalladay-Simpson, R. T. Howie, and E. Gregoryanz, Evidence for a new phase of dense hydrogen above 325 gigapascals, Nature (London) **529**, 63 (2016).

[9] D. Vollhardt and P. Wölfle, *The Superfluid Phases of Helium 3* (Taylor & Francis, London, 1990).

[10] A. Schmitt, *Introduction to Superfluidity* (Springer, Cham, 2015).

[11] L. Henry, M. Mezouar, G. Garbarino, D. Sifré, G. Weck, and F. Datchi, Liquid–liquid transition and critical point in sulfur, Nature (London) **584**, 382 (2020).

[12] Y. Katayama, T. Mizutani, W. Utsumi, O. Shimomura, M. Yamakata, and K. Funakoshi, A first-order liquid–liquid phase transition in phosphorus, Nature (London) **403**, 170 (2000).

[13] Y. Katayama, Y. Inamura, T. Mizutani, M. Yamakata, W. Utsumi, and O. Shimomura, Macroscopic separation of dense fluid phase and liquid phase of phosphorus, Science **306**, 848 (2004).

[14] J. N. Glosli and F. H. Ree, Liquid-Liquid Phase Transformation in Carbon, Phys. Rev. Lett. **82**, 4659 (1999).

[15] V. V. Brazhkin, S. V. Popova, and R. N. Voloshin, Pressure-temperature phase diagram of molten elements: selenium, sulfur and iodine, Phys. B (Amsterdam, Neth.) **265**, 64 (1999).

[16] D. Plašienka, P. Cifra, and R. Martoňák, Structural transformation between long and short-chain form of liquid sulfur from ab initio molecular dynamics, J. Chem. Phys. **142**, 154502 (2015).

[17] V. Holten and M. A. Anisimov, Entropy-driven liquid–liquid separation in supercooled water, Sci. Rep. **2**, 713 (2012).

[18] P. Gallo, K. Amann-Winkel, C. A. Angell, M. A. Anisimov, F. Caupin, C. Chakravarty, E. Lascaris, T. Loerting, A. Z. Panagiotopoulos, J. Russo, J. A. Sellberg, H. E. Stanley, H. Tanaka, C. Vega, L. Xu, and L. G. M. Pettersson, Effect of Hydrogen Bonds on the Thermodynamic Behavior of Liquid Water, Phys. Rev. Lett. **73**, 1632 (1994).

[19] M. Duška, Water above the spinodal, J. Chem. Phys. **152**, 174501 (2020).

[20] F. Caupin and M. A. Anisimov, Thermodynamics of supercooled and stretched water: Unifying two-structure description and liquid-vapor spinodal, J. Chem. Phys. **151**, 034503 (2019).

[21] P. H. Poole, F. Sciortino, U. Essmann, and H. E. Stanley, Phase behavior of metastable water, Nature (London) **360**, 324 (1992).

[22] V. Holten, J. C. Palmer, P. H. Poole, P. G. Debenedetti, and M. A. Anisimov, Two-state thermodynamics of the ST2 model for supercooled water, J. Chem. Phys. **140**, 104502 (2014).

[23] P. G. Debenedetti, F. Sciortino, and G. H. Zerze, Second critical point in two realistic models of water, Science **369**, 289 (2020).

[24] J. W. Biddle, R. S. Singh, E. M. Sparano, F. Ricci, M. A. González, C. Valeriani, J. L. F. Abascal, P. G. Debenedetti, M. A. Anisimov, and F. Caupin, Two-structure thermodynamics for the TIP4/2005 model of water covering supercooled and deeply stretched regions, J. Chem. Phys. **146**, 034502 (2017).

[25] P. G. Debenedetti, One substance, two liquids? Nature (London) **392**, 127 (1998).

[26] T. J. Longo and M. A. Anisimov, Phase transitions affected by natural and forceful molecular interconversion, J. Chem. Phys. **156**, 084502 (2022).

[27] F. Caupin and M. A. Anisimov, Minimal Microscopic Model for Liquid Polyamorphism and Waterlike Anomalies, Phys. Rev. Lett. **127**, 185701 (2021).

[28] G. E. Sauer and L. B. Borst, Lambda transition in liquid sulfur, Science **158**, 1567 (1967).

[29] R. Bellissent, L. Descotes, and P. Pfeuty, Polymerization in liquid sulphur, J. Phys.: Condens. Matter **6**, A211 (1994).

[30] V. F. Kozhevnikov, W. B. Payne, J. K. Olson, C. L. McDonald, and C. E. Inglefield, Physical properties of sulfur near the polymerization transition, J. Chem. Phys. **121**, 7379 (2004).

[31] A. V. Tobolsky and A. Eisenberg, Equilibrium polymerization of sulfur, J. Am. Chem. Soc. **81**, 780 (1959).

[32] A. Eisenberg and A. V. Tobolsky, Equilibrium polymerization of selenium, J. Polym. Sci. **46**, 19 (1960).

[33] N. A. Shumovskyi, T. J. Longo, S. V. Buldyrev, and M. A. Anisimov, Modeling fluid polyamorphism through a maximum-valence approach, Phys. Rev. E **106**, 015305 (2022).

[34] E. Zaccarelli, S. V. Buldyrev, E. L. Nave, A. J. Moreno, I. Saika-Voivod, F. Sciortino, and P. Tartaglia, Model for Reversible Colloidal Gelation, Phys. Rev. Lett. **94**, 218301 (2005).

[35] R. J. Speedy and P. G. Debenedetti, The entropy of a network crystal, fluid and glass, Mol. Phys. **81**, 237 (1994).

[36] R. J. Speedy and P. G. Debenedetti, The distribution of tetravalent network glasses, Mol. Phys. **88**, 1293 (1996).

[37] E. Wigner and H. B. Huntington, On the possibility of a metallic modification of hydrogen, J. Chem. Phys. **3**, 764 (1935).

[38] P. A. Giguere, Bifurcated hydrogen bonds in water, J. Raman Spectrosc. **15**, 354 (1984).

[39] B. J. Alder and T. E. Wainwright, Studies in molecular dynamics. I. general method, J. Chem. Phys. **31**, 459 (1959).

[40] D. C. Rapaport, *The Art of Molecular Dynamics Simulation*, 2nd ed. (Cambridge University, Cambridge, England, 2004).

[41] S. V. Buldyrev, Application of discrete molecular dynamics to protein folding and aggregation, in *Aspects of Physical Biology*, Lecture Notes in Physics, Vol. 752, edited by G. Franzese and M. Rubi (Springer-Verlag, Berlin, 2009), pp. 97–132.

[42] H. J. C. Berendsen, J. P. M. Postma, W. F. van Gunsteren, A. DiNola, and J. R. Haak, Molecular-dynamics with coupling to an external bath, J. Chem. Phys. **81**, 3684 (1984).

[43] A. Skibinsky, S. V. Buldyrev, G. Franzese, G. Malescio, and H. E. Stanley, Liquid-liquid phase transitions for soft-core attractive potentials, Phys. Rev. E **69**, 061206 (2004).

[44] N. R. Fried, T. J. Longo, and M. A. An, Modeling fluid polyamorphism through a maximum-valence approach, J. Chem. Phys. **157**, 101101 (2022).

[45] Poole, Sciortino, Grande, Stanley, and Angell, Water: A tale of two liquids, Chem. Rev. **116**, 7463 (2016).

[46] K. H. Kim, K. Amann-Winkel, N. Giovambattista, A. Späh, F. Perakis, H. Pathak, M. L. Parada, C. Yang, D. Mariedahl, T. Eklund, T.. J. Lane, S. You, S. Jeong, M. Weston, J. H. Lee, I. Eom, M. Kim, J. Park, S. H. Chun, P. H. Poole *et al.*, Experimental observation of the liquid-liquid transition in bulk supercooled water under pressure, Science **370**, 978 (2020).

[47] P. Bolhuis, M. Hagen, and D. Frenkel, Isostructural solid-solid transition in crystalline systems with short-ranged interaction, Phys. Rev. E **50**, 4880 (1994).